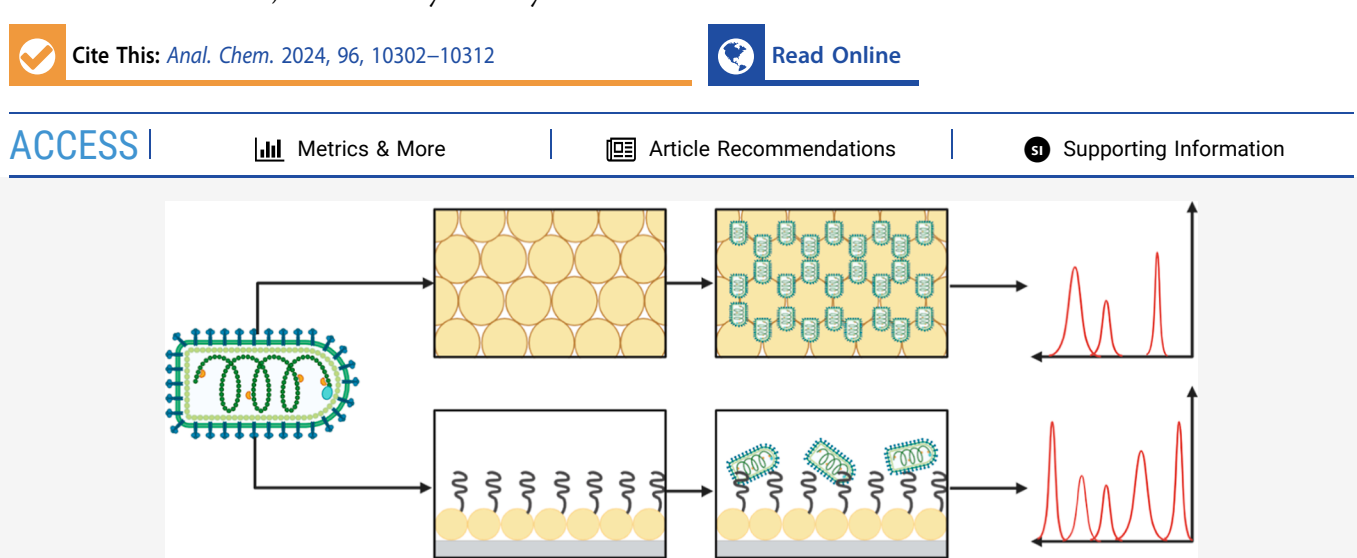


pubs.acs.org/ac Article

Label-Free Detection of Virus-like Particles with Surface-Enhanced Raman Spectroscopy through Analyte Localization and Polymer-Enabled Capture

Published as part of Analytical Chemistry virtual special issue "Celebrating 50 Years of Surface Enhanced Spectroscopy".

Cassandra L. Wouters, Mahmoud Matar Abed, Timmy B. Nguyen, Clarice E. Froehlich, Punarbasu Roy, Theresa M. Reineke, and Christy L. Haynes*



ABSTRACT: Virus detection is highly important; the last several years, since the onset of the SARS-CoV-2 pandemic, have highlighted a weakness in the field: the need for highly specialized and complex methodology for sensitive virus detection, which also manifests as sacrifices in limits of detection made to achieve simple and rapid sensing. Surface-enhanced Raman spectroscopy (SERS) has the potential to fill this gap, and two novel approaches to the development of a detection scheme are presented in this study. First, the physical entrapment of vesicular stomatitis virus (VSV) and additional virus-like particles through substrate design to localize virus analytes into SERS hotspots is explored. Then, the use of nonspecific linear polymers as affinity agents to facilitate polymer-enabled capture of the VSV for SERS detection is studied. Quantitative detection of the VSV is achieved down to 10^1 genetic copies per milliliter with an R^2 of 0.987 using the optimized physical entrapment method. Physical entrapment of two more virus-like particles is demonstrated with electron microscopy, and distinctive SERS fingerprints are shown. This study shows great promise for the further exploration of label-free virus detection methods involving thoughtful substrate design and unconventional affinity agents.

1. INTRODUCTION

In light of the SARS-CoV-2 pandemic, it is easy to understand the urgency and necessity of sensitive virus detection. Viruses are not only important to study because of their pathogenic potential but also are critical in the burgeoning field of virus-based therapeutics. Oncolytic applications of viral therapies are also being explored for their ability to selectively attack cancerous cells. Vesicular stomatitis virus (VSV) is a bullet-shaped, enveloped, single-stranded RNA virus in the *Rhabdoviridae* family which has recently shown promise as a therapeutic to preferentially target cancerous tumors (Figure 1).¹

The current gold standard for virus detection is the polymerase chain reaction (PCR), which is neither rapid nor

simple and requires specialized knowledge to conduct.² Further, PCR is irrelevant for virus-like particles lacking nucleic acid cargo. These challenges are common across sensing schemes for many biological analytes; however, surface-enhanced Raman scattering (SERS) is a method that can overcome these challenges and has been used for detection

Received: February 28, 2024
Revised: May 17, 2024
Accepted: June 4, 2024
Published: June 14, 2024





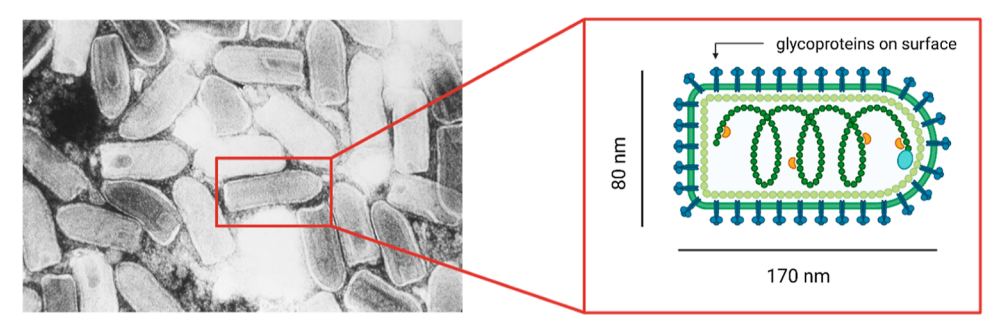


Figure 1. VSV structure. An electron micrograph of the VSV structure (by the Centers for Disease Control and Prevention, public domain) with callout of a single virion, including size dimensions and some surface information. Created with BioRender.com.

of biologically relevant small molecules, viruses, and bacteria.^{3,4} For example, bacteria have been detected and accurately classified by species at the single-cell level using Raman microspectroscopy coupled with chemometric analysis.^{5,6} Despite the precedent work, applying SERS to virus detection remains a relatively unexplored pathway ripe for innovation, having only taken off in the past few years, with much literature emerging since the onset of the COVID-19 pandemic.^{7,8}

Vibrational spectroscopy gives chemical fingerprint information because the molecular vibrational modes manifest as spectral features, reflecting the vibrational character of each functional group. In Raman spectroscopy, molecular vibrations that affect molecular polarizability are active. Raman scattering is the inelastic scattering of photons and is a rare phenomenon which occurs naturally for only 1 in 10⁷ scattered photons. The mechanism behind the Raman signal intensity is controlled by the strength of the dipole induced by the molecular vibration, which depends on the polarizability of the molecule and the electric field. Because Raman scattering occurs infrequently, it produces inherently low signals; plasmonic enhancement of Raman scattering is needed to use Raman spectroscopy as a reliable and practically useful analytical technique. SERS allows for Raman signal gains of up to 10¹⁰ by manipulating both the polarizability of the molecule and the electric field. Electromagnetic enhancement is facilitated by exciting a localized surface plasmon resonance (LSPR) on noble metal nanostructures and contributes up to 108 to the signal enhancement. The LSPR depends on the dielectric constant of the material as well as the size, shape, and spacing of the nanoscale features. 10 When performing SERS, it is therefore important that the λ_{max} of the substrate extinction (absorption plus scattering, indicating the excited LSPR) is of similar energy to the laser wavelength so that the plasmon will be effectively excited, and the electromagnetic fields necessary for surface enhancement are generated.

Plasmonic substrates can be developed in a variety of forms for SERS applications, mainly divided between colloidal nanoparticles and substrate-bound nanostructures. Metal film over nanospheres (FONs) are one such reproducible and easily fabricated substrate, which generally have enhancement factors around 10⁵, are shelf-stable, and allow for the use of liquid-phase analytes without dilution. The LSPR is tuned by changing the film thickness, the size of nanostructures and any gaps, and the plasmon-supporting material. Other forms of nanoscale lithography are also popular, as are colloidal metal nanoparticles as substrates. Another consideration when developing SERS detection schemes is whether to measure the molecular fingerprint of the analyte (intrinsic SERS) or to use a Raman tag, which may aid in the detection

of weak scatterers (extrinsic SERS). Extrinsic SERS is easy to analyze but does not give direct information about the analyte, while spectra obtained by intrinsic SERS can be definitively assigned and interpreted in relation to the analyte. Affinity agents are often used to enable intrinsic SERS to help bring the analytes into enhancement zones or provide selectivity, but they often have peaks in overlapping wavenumber regions as the analytes, thus visually complicating the spectra. Thus, the experimental design of intrinsic SERS for sensing must consider the balance between complex data analysis and the potential difficulty in spectral congestion.

This work will show that SERS can be exploited to sensitively detect VSV as a proof-of-concept with preliminary explorations into the detection of additional virus-like particles. Two strategies will be employed: (i) localization of the analyte in the enhancement zones by modeling the nanostructured gaps on the substrate surface to fit the dimensions of the analyte and (ii) capture by nonspecific linear polymers as affinity agents. The small size of individual virions allows for the use of micro- and nanoscale features to facilitate analyte localization in substrate gaps while still supporting plasmonic resonance. The localization is driven by physical forces like evaporation of the analyte solution post-incubation into the virus-sized gaps engineered in the substrate. This novel strategy will offer the advantage of only having the analytes' vibrational modes interpreted in the spectra.

This work aims to advance this field not only by detecting novel analytes but also by exploring multiple uncommon strategies for label-free detection: the physical entrapment of analytes and the use of promiscuous linear polymer affinity agents. Though compelling, it may be disadvantageous to rely on physical entrapment alone. As such, passive localization will be compared with the use of nontraditional affinity agents, such as linear polymers. These polymers do not have a specific affinity to the VSV but instead contain multiple functional groups that will promote noncovalent interactions with the analyte while being covalently attached to the substrate surface. 22,23 Utilizing chemical attraction could bring more analyte to the enhanced substrate regions, though it will complicate the data with polymer vibrational fingerprints. The physical entrapment of the VSV on the substrate surface across a wide range of concentrations will be presented following preliminary data using virus-sized model nanobeads. Two linear polymers and two methods for the interaction of the analyte with the polymer are explored with VSV detection over a range of concentrations. Overall, this work reveals that the physical entrapment method is preferable and allows for VSV detection at low concentrations and for quantitation.

2. MATERIALS AND METHODS

2.1. FON Fabrication. FONs were fabricated following previously published protocols. ^{14,22,23} In brief, silicon wafers were cleaned using a piranha solution to remove metals and contaminants from the surface. Nonfunctionalized silica nanospheres (Bangs Laboratories, Inc., Fishers, IN) of desired diameter (500 or 1000 nm) were resuspended in Milli-Q water and then drop-cast onto the clean silicon and allowed to dry in ambient conditions. A Denton 502B vacuum deposition system was used to deposit rough gold films onto the selfassembled monolayer of silica spheres at a deposition rate of ~2 Å/s. Substrates were mounted onto a metal disk with vacuum-safe polyimide tape. Gold (99.999% pure, Kurt J. Lesker Co., Jefferson Hills, PA) film deposition was monitored by a quartz crystal microbalance. Extinction spectroscopy was performed by using an Ocean Optics USB2000 reflectance fiber optic spectrometer on each substrate after calibration with a reflective gold blank.

2.2. Polymer Synthesis. All polymers in this work were synthesized by reversible addition-fragmentation chain transfer (RAFT) polymerization.²⁴ Poly-N-(2-aminoethyl)methacrylamide (pAEMA) and poly-2-hydroxyethyl methacrylate (pHEMA) were synthesized from commercially available monomers [Polysciences, Inc. (Warrington, PA) and Sigma-Aldrich (St. Louis, MO), respectively] (Figure S1). To the monomer solutions, initiator 4,4'-azobis(4-cyanovaleric acid) and chain transfer agent 4-cyano-4-(propylsulfanylthiocarbonyl) sulfanylpentanoic acid were added.²³ Details are shown in Figure S1. To prepare the products for size exclusion chromatography (SEC) and nuclear magnetic resonance (NMR), they were run through dialysis and lyophilization. An Agilent 1260 Infinity Quaternary LC system with Eprogen columns [CATSEC1000 (7 μ m, 50 \times 4.6), CATSEC100 (5 μ m, 250 × 4.6), CATSEC300 (5 μ m, 250×4.6), and CATSEC1000 (7 μ m, 250×4.6)] was used for SEC to obtain the molecular weight of the products with a Wyatt HELEOS II light scattering detector ($\lambda = 662 \text{ nm}$) and an Optilab rEX refractometer at 658 nm. To confirm the structure, AX-400 ¹H NMR at the UMN Department of Chemistry NMR laboratory was used. The results of these characterizations are shown in Table S1.

2.3. Physical Entrapment of Virus-Sized Nanobeads. To model the dimensions of the VSV, 68 nm-diameter polystyrene and 177 nm-diameter silica (Bangs Laboratories, Inc., Fishers, IN) nanobeads were incubated on FONs. As a preparation, the silica nanobeads were centrifuged and resuspended in Milli-Q water several times to remove surfactant. The polystyrene nanobeads were used without preparation. Twenty μL of the nanobead solutions were added to FONs and allowed to dry overnight. Samples were then mounted on scanning electron microscopy (SEM) stubs and coated with 2 nm-thick Pt. SEM was performed at a 5.0 kV accelerating voltage with secondary electron detectors. The FONs templated with 1000 nm-diameter spheres were imaged on a JEOL 6500 scanning electron microscope, while the FONs templated with 500 nm-diameter spheres were imaged on a Hitachi SU8230 scanning electron microscope.

2.4. Physical Entrapment of VSVs. To perform SERS on a wide range of VSV concentrations, 1:100 serial dilutions from the stock VSV solution (10¹¹ genetic copies/mL) down to 10¹ genetic copies/mL were prepared. Each VSV solution was added to a FON in triplicate, incubated at room temperature

for 2 h, and then dried with N_2 gas. SERS measurements are described below.

For the imaging of VSV on a FON surface, VSV solutions were added to FONs and incubated for 2 h at room temperature and dried with $\rm N_2$ gas. After mounting on SEM stubs with conductive carbon tape, they were immediately coated with 1 nm of Pt using an Ion Beam Sputterer TM200S (VCR Group, Inc.). SEM was performed at a 5.0 kV accelerating voltage with secondary electron detectors on the Hitachi SU8230 scanning electron microscope.

VSV samples and an appropriate buffer were provided by Boehringer Ingelheim (Ridgefield, CT). The provided samples were genetically modified to not contain infective RNA. For the other virus-like particles, the same physical entrapment SERS and SEM protocols were followed. Adeno-associated virus empty capsids were purchased from PROGEN INC. (Wayne, PA). The virus-like particle VLP-N5213 was purchased from ACROBiosystems (Newark, DE). Dilutions of AAV and VLP-N5213 were made in 1X DPBS (Corning Inc., Corning, NY).

2.5. Polymer-Enabled Capture. 2.5.1. Preincubating vs Premixing. Polymer-enabled capture of the VSVs can be done by first incubating the polymer on the substrate surface, followed by drying, and then the introducing the analyte onto the polymer-functionalized FON, which will be referred to as preincubating. One mM pHEMA or 1 mM pAEMA in water was dropped onto the FON surface, incubated for 2 h at room temperature, and then dried with N_2 gas. The VSV stock solution was added to the surface for 2 h at room temperature and then dried with N_2 gas. SERS measurements are described in the following Materials and Methods section.

The premixing method of polymer-enabled capture involved first combining equal parts of 1 mM pAEMA or 1 mM pHEMA with the stock VSV. This mixture was stirred on a rocking shaker for 2 h at room temperature and then added to the nonfunctionalized FON. The polymer-VSV mixture was allowed to incubate on the FON for 2 h at room temperature and then dried with N_2 gas. SERS measurements are described in the following Materials and Methods section.

2.5.2. Premixing pAEMA with a Range of VSV Concentrations. To perform SERS on a wide range of VSV concentrations, the premixing method was used. The VSV solutions were prepared as 1:100 serial dilutions from the stock solution (10¹¹ genetic copies/mL) down to 10¹ genetic copies/mL. A 50:50 mixture of each VSV solution was individually mixed with 1 mM pAEMA for 2 h at room temperature on a rocking shaker. Each VSV solution was added to a FON in triplicate, incubated at room temperature for 2 h, and then dried with N₂ gas. SERS measurements are described in the following Materials and Methods section.

2.6. SERS Experiments. SERS measurements were recorded using a SnRI Sierra system (Snowy Range Instruments, Laramie, WY) and an XYZ sample stage and a 785 nm excitation laser. Samples were mounted to the stage and measured at five different spots on the substrate to obtain five spectra per sample. 38 mW laser power and 15 s integration time were used unless otherwise noted. The data were then baselined with a program adapted from an open-source algorithm (BubbleFill). Baselined results for each experimental condition were then averaged. Plots were created in Origin 2018 (OriginLab). Principal component analysis (PCA) was performed on baselined data to visualize variance between the different experimental conditions and was implemented

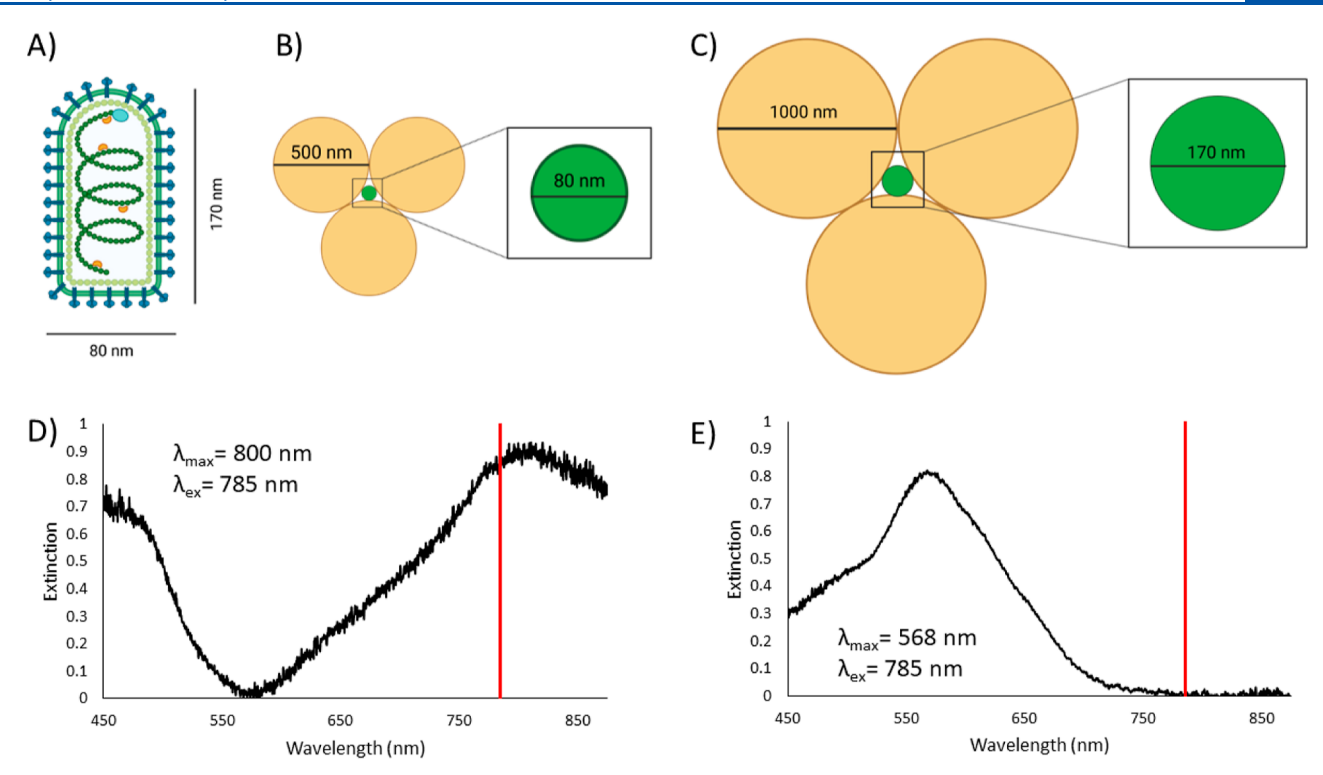


Figure 2. Physical entrapment geometric considerations. (A) illustrates the morphology and dimensions of VSV. (B,C) show geometric representations of the gap created at the intersection of three nanospheres with a nanobead (green) sized to fill the aforementioned gap. The ideal diameter for the nanospheres to accommodate an 80 nm-diameter bead, which corresponds to the small dimension of the VSV, is 500 nm (B). The ideal diameter for the nanospheres to accommodate a 170 nm-diameter bead, which corresponds to the long dimension of the VSV, is 1000 nm. (D) shows a representative extinction spectrum for a FON made with 500 nm-diameter nanospheres, with a $\lambda_{\rm max}$ at 800 nm. (E) shows a representative extinction spectrum for a FON made with 1000 nm-diameter nanospheres, with a $\lambda_{\rm max}$ at 568 nm. The 500 nm-diameter nanosphere-based FON can therefore support greater electromagnetic signal enhancement when using a 785 nm excitation laser (represented by the red vertical line in parts D and E). Created with BioRender.com.

using scikit-learn in Python. Outlier analysis for the calibration curves was performed using GraphPad's ROUT method with a maximum false discovery rate (Q) of 1% and can detect multiple outliers from a data set, eliminating a maximum of 30% of a data set. ²⁶

3. RESULTS

3.1. Physical Entrapment. Determining the viability of the simplest intrinsic detection scheme was done first using model nanobeads as stand-ins for the VSV sample, which was available only in limited quantities. VSV is bullet-shaped (Figure 2a),²⁷ thus one nanobead was used to model the short dimension (80 nm) and one for the long dimension (170 nm) of the VSV. With the goal of localizing the VSVs in the gaps between the nanospheres comprising the substrate surface, the ideal sizes of the nanospheres were geometrically determined to be 500 nm to fit the short dimension of the VSV (Figure 2b) and 1000 nm to fit the long dimension of the VSV in the nanosphere array gaps (Figure 2c). However, the sizes of the templating nanospheres have implications for the utility of the SERS substrate due to the effects on the LSPR. FONs are generally highly tunable, and there is typically a positive correlation between the sphere size and the LSPR wavelength, whereas for the thickness of the gold film and the LSPR wavelength, the correlation is negative. 22 Therefore, the gold thickness was adjusted when using the 500 nm spheres to have the maximum absorbance around 785 nm, the wavelength of the excitation laser (Figure 2d). With the 1000 nm spheres, however, the LSPR was not tunable through adjustments of the

gold thickness (Figures S2 and 2e). This unexpected result meant that the 1000 nm substrates were not useful for this project as the majority of the SERS enhancement comes from the LSPR, and the available laser was fixed at 785 nm, despite the geometry of this substrate being able to accommodate both dimensions of the VSV. All SERS experiments therefore utilized the 500 nm FONs, thus focusing on VSV capture based on the smaller dimension.

As a proof-of-concept demonstration of physical entrapment, the model nanobeads were incubated on the surfaces of the 500 nm-diameter FONs and the 1000 nm-diameter FONs for 2 h and dried. SEM was used to visualize nanobead localization on the FONs (Figure 3). In both cases, the bare FONs show that the monolayered nanosphere array packs with good uniformity over a large area (Figure 3a,b, respectively). Figure 3c shows that the long-dimension model nanobeads settle in the gaps and crevices between the 500 nm-diameter nanospheres despite the smallest footprint of the gaps not being large enough to fully encapsulate the beads, which should still allow for substantial LSPR effects. The largedimension nanobeads are also shown packing in the 1000 nmdiameter FON crevices, suggesting that the relative closeness of the VSV to both the 500 nm-diameter and 1000 nmdiameter high curvature features on the FONs would be similar (Figure 3d). In Figure 3e, the small-dimension nanobeads on the 500 nm-diameter FON are packed in the gaps and crevices very similarly to the way the large-dimension beads are packed on the 1000 nm-diameter FONs, indicating that substrates that are ideally designed for one size of nanobead exhibit packing of

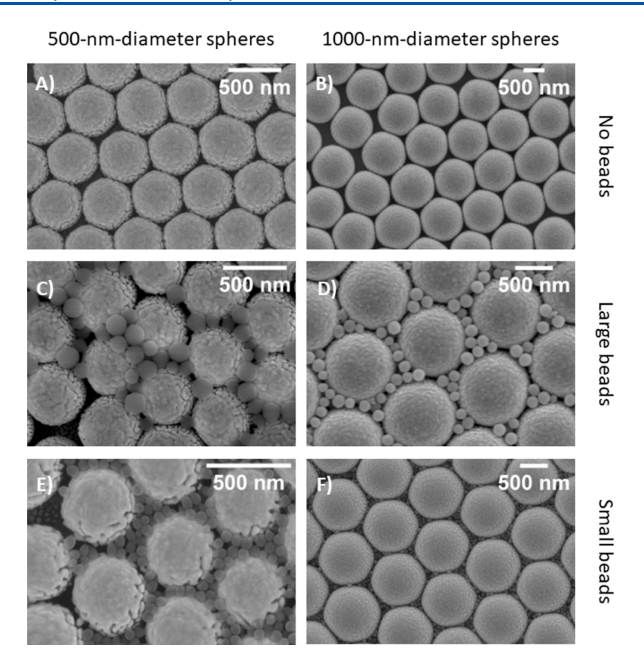


Figure 3. SEM images of model nanobeads localized on FON surfaces. (A) shows the bare 500 nm-diameter FON surface. (B) shows the bare 1000 nm-diameter FON surface. (C) shows the large beads and (E) shows the small beads packed into the 500 nm-diameter nanosphere array, corresponding to the illustration in Figure 2B. (D,F) show the 1000 nm-diameter FONs with the large and small beads, respectively, corresponding to the illustration in Figure 2C.

that nanobead into ordered gaps and crevices and not just holes. The small-dimension nanobeads have a large size differential from the 1000 nm spheres, resulting in many nanobeads packing into each gap (and many not being within close proximity of the plasmonic surface; Figure 3f). Overall, based on both the tunability of the LSPR of the 500 nm-diameter substrates and the ability of both sizes of nanobead to sit in the gaps and crevices of the FON, work proceeded using the 500 nm-diameter FON for all further experimentation.

Having demonstrated the physical entrapment technique using the model nanobeads with size features relevant to VSV, SERS detection of VSV was undertaken. To our knowledge, there were no prior examples in the literature of the fingerprint of VSV with SERS. Thus, a characteristic SERS spectrum of the undiluted sample alongside hypothesized vibrational band assignments is shown in Figure 4 and Table 1, respectively. Generally, the SERS signals seen are likely attributable to the surface glycoproteins.

Based on this fingerprint spectrum, a range of concentrations of VSV were tested. In Figure 5, the SERS spectra for the stock concentration of VSV (in black) and hundred-fold serial dilutions through 10¹ genetic copies per milliliter are shown. There is a clear difference between the group of the three highest and the group of the three lowest concentrations, with larger signals accompanying the higher concentrations of analyte. For some of the vibrational modes, the signals scale linearly against the logarithm of the concentration, with an R² of 0.987 (Figure 6). For instance, the peak at 986 cm⁻¹ shift may come from the aromatic amino acids tryptophan and phenylalanine or C–C stretching.²⁸ This linear scaling may indicate that their presence on the surface of the VSV is important to the SERS detection and that the glycoprotein (containing numerous phenylalanine and tryptophan residues) is in close proximity to the substrate as it serves as a conduit

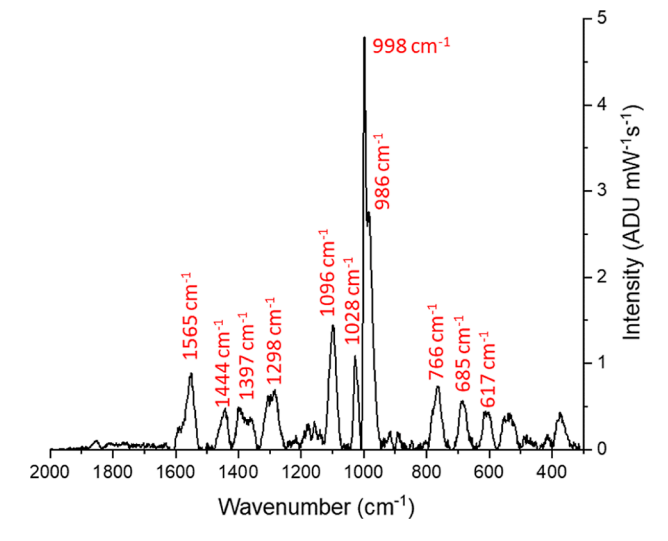


Figure 4. VSV SERS fingerprint spectrum of stock VSV solution deposited on a FON. The identified peaks have hypothesized Raman shift assignments in Table 1.

Table 1. Hypothesized Raman Shift Assignments for VSV

| Table 1. Hypothesized Raman Shift Assignments for VSV | |
|---|---|
| Raman shift (cm ⁻¹) | possible peak assignments |
| ~617 | N-H (bending) ^{30,31} |
| ~685 | C-S (stretching) ^{31,32} |
| ~766 | Trp (ring breathing) ^{30,31,33} |
| ~986 | C-C (stretching) ^{32,33} |
| ~998 | Ph (ring breathing) ^{30,31} |
| ~1028 | Trp, ²⁸ Phe, ³¹ Arg, ³¹ Gly, ³¹ Ile ³¹ |
| ~1096 | C-N (stretching) ^{30,31,33} |
| ~1298 | C-H (deformation), ³⁰ imidazole (ring stretching) ³³ |
| ~1397 | Trp indole ring ³² |
| ~1444 | CH ₂ /CH ₃ (stretching) ^{31,32} |
| ~1565 | Trp (ring stretching) ^{30,31,33} |
| | |
| 10 ¹ gc/ml | |
| 10 ³ gc/ml | 1 |
| 10 ⁵ gc/ml | |
| 10 ⁷ gc/ml | |

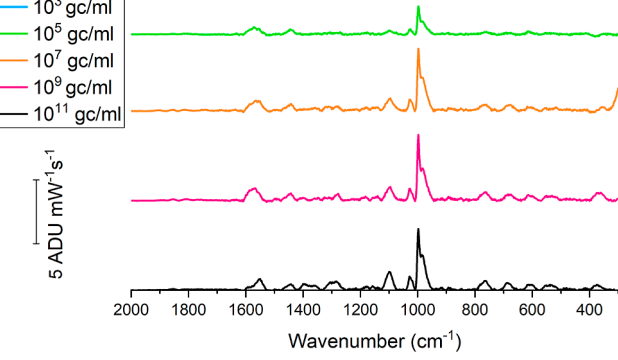


Figure 5. SERS of physically entrapped VSV over a wide range of concentrations from 10^{11} to 10^{1} genetic copies/mL (gc/mL). There is a clear trend that the lower concentrations of analyte have smaller peaks. The highest concentration of VSV (10^{11}) is shown in black at the bottom of the graph, with each spectrum being 100 times less concentrated than the one below it. The pink spectrum is 10^9 , the orange spectrum is 10^7 , the green spectrum is 10^5 , the blue spectrum is 10^3 , and the purple spectrum is 10^1 gc/mL. Spectra are offset vertically for easier visualization.

for viral introduction into host cells.²⁹ The reason for the linearity on the logarithmic scale is likely because the

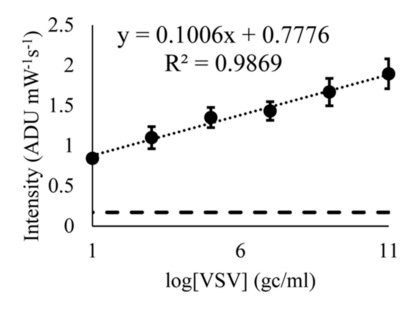


Figure 6. Calibration curve for the 986 cm $^{-1}$ Raman shift band for the physically entrapped VSV. The error bars shown are the standard error of the mean. The flat dashed line is the calculated LOD. There is a positive linear relationship between the peak intensity and the logarithm of the concentration of the VSV, characterized by an R^2 of 0.987.

increasing concentration of the analyte increasingly occupies the sites of significant SERS enhancement, such that the effect reaches a maximum.

Additionally, the peak at the 766 cm^{-1} shift also follows a linear trend, with an R^2 of 0.948 (Figure S3). This signal may come from a tryptophan ring breathing mode and further supports the idea that a higher concentration of the analyte results in more of the VSV surface glycoprotein in the SERS hotspots. The horizontal dashed line in Figures 6 and S3 represents the limit of detection (LOD), calculated as three times the average noise in a Raman silent region of the spectra. Clearly, even with the low end of the explored concentrations of the analyte, the signals exceed the LOD, showing that the VSV is detectable at around 10^1 genetic copies per milliliter and potentially lower concentrations beyond the tested range.

Overall, the physical entrapment method worked well for VSV and has the potential to be applied to a range of virus-like particles and viruses that exist in accommodatable size ranges when designing FONs (Table S2). The simplicity of this detection scheme is enticing as a low LOD was attained for the intrinsic detection of the bioanalyte without the need for an affinity agent. Additionally, results are comparable to other detection methods for viruses like PCR, which has an LOD of around 10² genetic copies/mL for COVID testing. Thus, SERS, making use of physical entrapment, holds potential for development into clinical or environmental assays for virus detection, especially for virus-like particle detection where the nucleic acid cargo has been removed to facilitate loading with alternate cargo.

The physical entrapment method is further supported by the visualization of virus-like particles on the FON surface, shown in Figure 7. The particles rest in the gaps and crevices between the template spheres. Before SEM analysis, the samples were platinized to help with sample charging, which also resulted in the film left from the buffer appearing in the images (especially apparent in Figure 7b). In Figure 7a, the bullet shape of the VSV is clearly shown, and Figure 7b shows many VSV particles seated in the gaps between the 500 nm-diameter spheres. Figure 7c shows a VLP-N5213 particle entrapped between the FON's template nanospheres. AAV, though much smaller than the VSV and VLP-N5213, packs into the FON gaps well and more closely resembles the model nanobead packing due to its roughly spherical shape (Figure 7d). The same behavior of localization in the nanogaps is shown for all three virus-like particles, providing strong support for the utility of FON-based physical entrapment for a broad range of virus analytes.

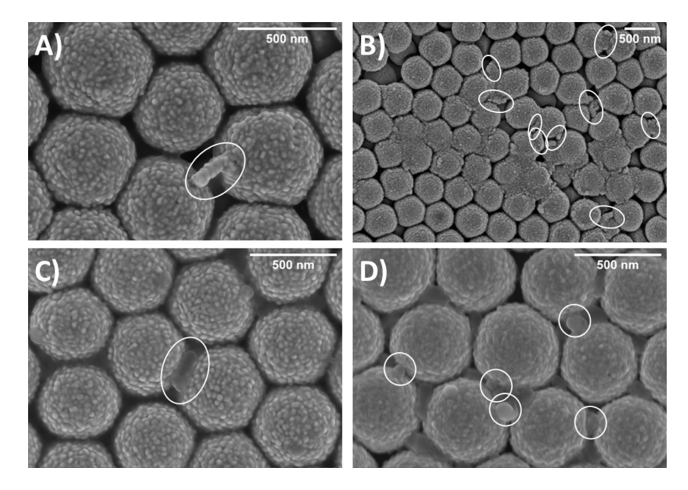


Figure 7. SEM images of VSV, VLP-N5213, and AAV on FONs, platinized to minimize charging. Many of the virus-like particles are circled for added clarity. (A) shows the characteristic bullet shape of the VSV resting in a gap between 500 nm-diameter spheres. (B) shows many VSVs localized in the FON crevices. (C) shows VLP-5213 between 500 nm-diameter spheres. (D) shows multiple AAVs in the 500 nm-diameter sphere array.

Having demonstrated that physical entrapment functions similarly among the three virus-like particles, comparisons between the SERS spectra were examined. The fingerprints for AAV and VLP-N5213 are shown in Figure 8. Comparison with the VSV fingerprint (Figure 8) clearly shows the visual differences between all three analytes. Additionally, the PCA shows that the different analytes cluster distinctly (Figures S4–S6). KMeans analysis reveals that the clusters of VSV and a

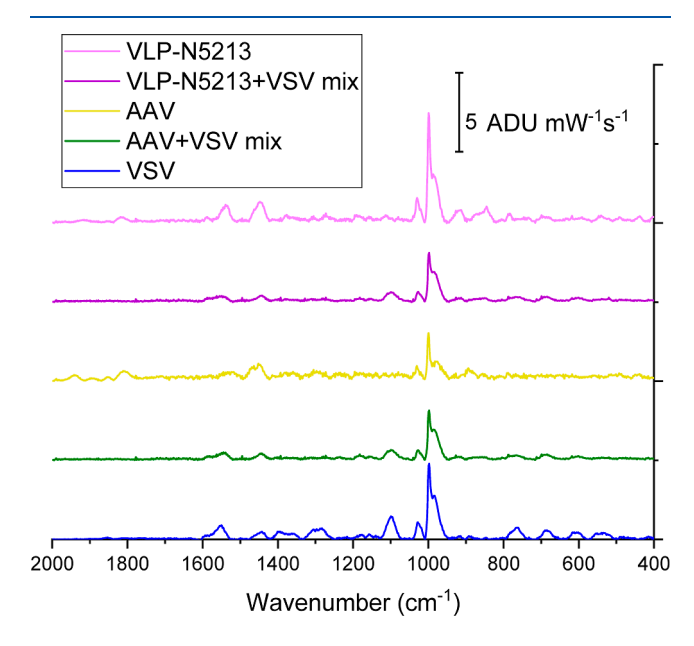


Figure 8. SERS spectra of AAV and VLP-N5213 individually and mixed with VSV. Spectra are offset for easier visualization. The pink spectrum (top) is that of VLP-N5213 at 50 μ g/mL. The purple spectrum is 50 μ g/mL VLP-N5213 mixed with 10¹¹ gc/mL VSV. The yellow spectrum is 10¹¹ capsids/mL AAV. The green is 10¹¹ capsids/mL AAV mixed with 10¹¹ gc/mL VSV. The blue spectrum is 10¹¹ gc/mL VSV. The fingerprints for the AAV and VLP-N5213 are distinct from both VSV and each other. The mixture of AAV and VSV reflects the character of each individual analyte. The same is true of the mixture of VLP-N5213 and VSV.

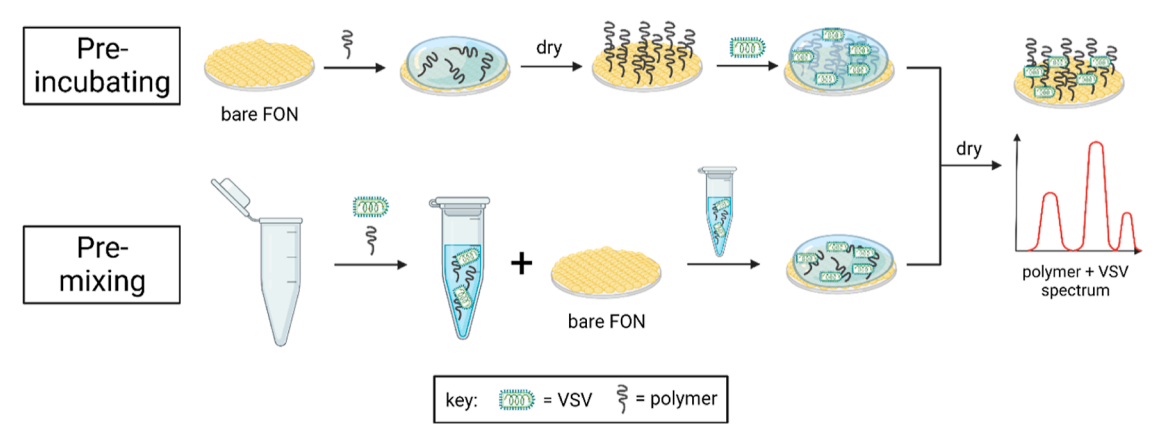


Figure 9. Schematic of preincubating and premixing methods. For preincubating, the polymer solution is added to the bare FON and dried, followed by the addition of the analyte. For premixing, the VSV analyte and polymer are mixed together before being added to the FON surface. In both cases, the spectra are measured after drying (the previous step). Created with BioRender.com.

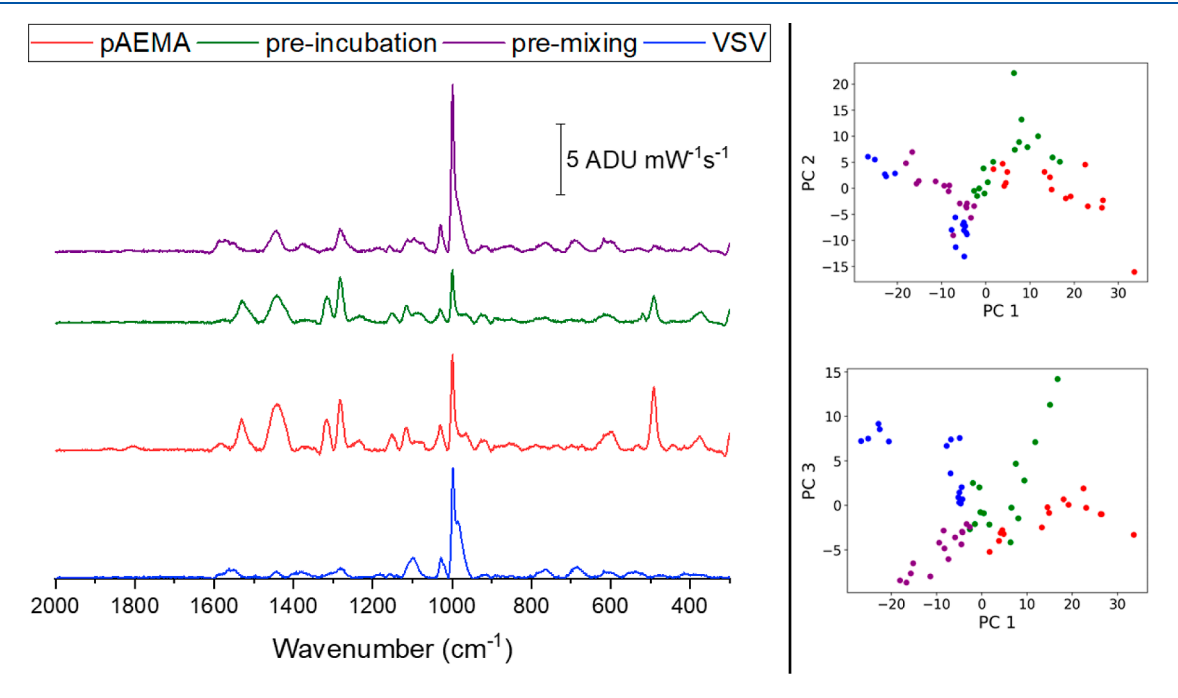


Figure 10. Premixing versus preincubation methods for pAEMA and VSV. For both the spectra and the PCA, the red is pAEMA alone, the green is the preincubation method of pAEMA and VSV, the purple is the premixing method of pAEMA and VSV (top), and the blue is VSV alone (bottom). The preincubation method primarily shares characteristics with the polymer, whereas the premixing method is more similar to the VSV. Preincubation is inseparable from pAEMA, but premixing is separable from both the VSV and polymer with PCA.

lower concentration of VLP-N5213 for PC1 versus PC2 cluster with 94.8% accuracy (Figure S4). When VSV and AAV were added to the same FON for a multiplex trial, the resulting spectrum had character from each analyte and some features that overlapped (Figure S5). PCA shows that the mixture of the two analytes clustered with a slight overlap with the VSV cluster, while the AAV remained distinct for both PC1 vs PC2 and PC1 vs PC3 (Figure S5). The closeness of the mixture of AAV and VSV clusters to the VSV alone indicates that the spectra of the mixture are more similar to the VSV spectrum than that of the AAV. For the multiplexing of the VSV and VLP-N5213, the combination spectrum again shares character with each analyte (Figure S6). For example, the peak around 1100 cm⁻¹ shift from the VSV is seen in the combined spectrum, as is the peak around 925 cm⁻¹ shift from VLP-N5213, despite not being present in both analytes individually. The PCA of VSV and VLP-N5213, however, does not have a

distinct cluster for each analyte and the combination of the two (Figure S6). In fact, the VSV cluster is well-separated from the mixture, while the VLP-N5213 data points overlap with both the VSV and the combination when considering PC1 vs PC2. For PC2 versus PC3, the plot shows the overlap of all three clusters. Thus, VLP-N5213 and VSV are more spectrally similar than VSV and AAV. Overall, these data support our hypothesis that the physical entrapment detection scheme can be applied to a variety of viruses and virus-like analytes and results in distinct spectral fingerprints.

Physical entrapment of VSV for SERS detection was therefore achieved over a wide range of concentrations, and there is convincing physical and spectroscopic evidence to support the hypothesis of the entrapment of the appropriately sized analyte in the substrate's gaps. Regarding the power and limits of this method, a primary disadvantage is the limited range of electromagnetic field enhancement (and thus signal

enhancement) in SERS. Because of this decay, differentiation of viruses would be limited by what is on the surface of the viruses. This may mean that differentiation of closely related strains is not be feasible. However, not needing specialized affinity agents or primers is a major advantage of this technique. We clearly demonstrated the ability to detect multiple virus analytes with the same detection scheme. Additionally, this method is nondestructive, allowing for the potential to recover the analytes after detection for further analysis or use. This facile fabrication of stable substrates holds promise for similar bioanalytes for their label-free detection with localization in SERS hotspots.

3.2. Polymer-Enabled Capture. While exploring the impact of a FON-anchored linear polymer affinity agent, two methods of introducing the polymer and analyte were explored: preincubating and premixing, as depicted in Figure 9. The former involves subsequently incubating the polymer and the analyte with a drying step between the introductions. Premixing instead mixes the polymer and analyte together and incubates them first before adding the mixture to the substrate surface. Ultimately, in both cases, the substrate with the polymer and the analyte on the surface is incubated for 2 h, followed by drying and measuring. The polymers in this study and the VSV are expected to primarily interact through noncovalent intermolecular forces, especially hydrogen bonding, sites for which are available in the repeat units of both pHEMA and pAEMA. Additionally, they were synthesized with terminal trithiocarbonate groups to allow for anchoring to the gold substrate surface. The lack of specificity of the expected interactions between the polymer affinity agents and the virus is of interest because it may allow for future multiplexing and/ or the application of this detection scheme to a wide range of analytes. Previous studies indicated that the premixing method would likely be preferable, which results aligned with, as shown in Figure 10. This may be because the VSV can interact with more sites on the free polymer (i.e., the polymer repeat units capable of H-bonding), while the ends of the linear polymer may be the only accessible sites for intermolecular interaction when the polymer is first allowed to bind to the gold surface for preincubation. There is a high affinity for the FON surface and polymer through gold-thiol bonding, so it may pack tightly on the surface and cause the VSV to be farther from the enhanced electromagnetic field of the plasmonic substrate. The distance dependence of SERS enhancement is a well-known phenomenon, with SERS enhancement falling off quickly as a function of distance.³⁵ Thus, premixing may be the better method to bring the VSV close to the FON surface for maximum SERS enhancement.

The polymer and VSV unfortunately have peaks of interest in overlapping wavenumber regions of their respective spectra, complicating the interpretation of the spectra that are combinations of the affinity agent and analyte (Figure 10). When comparing the pAEMA spectrum to both the preincubating and premixing spectra, it is clear that the preincubating spectrum highly resembles the polymer spectrum, while the premixing spectrum has different primary peaks. However, the premixing spectrum is very similar to the VSV fingerprint spectrum. PCA was also used to visualize data clustering from class to class as a result of their sources of variance. PCA is an unsupervised machine learning method and thus does not require labeled input data, so if different experimental conditions do not have very different spectral variance sources, they will appear closer together and will

provide insight into this relationship. This qualitative analysis is helpful for the interpretation of spectrally congested data and understanding if the VSV analyte or the polymer affinity agent are more important or influential in our detection scheme. From the PCA, the pAEMA and the preincubating method are inseparable into clusters for both PC1 versus PC2 and PC1 versus PC3. The VSV and premixing, on the other hand, are distinctly clustered in PC1 versus PC3 and are separable from the preincubating and polymer spectra as well. Between the PCA clustering and the appearance of the premixing spectrum possessing more VSV character than polymer character, further studies were carried out using the premixing method.

It logically follows that the preincubating method would lead to more polymer character because the introduction of the polymer to the substrate surface first allows for the occupation of SERS hotspots by the gold-sulfur attachments of the pAEMA to the FON surface. The lack of differences seen for the preincubated spectrum and the polymer spectrum indicates that the VSV likely could not reach the enhancement zones in significant quantities. This is further supported by an additional study which lowered the polymer concentration 100-fold, resulting in the pAEMA and VSV combination spectrum having a lower signal-to-noise ratio for several of the characteristic Raman shift peaks, indicating that a 1 mM pAEMA concentration is appropriate (Figure S8). The pAEMA has a much higher affinity for the FON surface (through gold-thiol bonding) than the VSV does, such that the subsequent introduction of the analyte into the preassociated polymer-substrate surface does not interrupt the occupation of the enhancement zones by the polymer to be able to reliably detect the analyte.

Having determined the favorability of the premixing method, we then compared two candidate linear polymer affinity agents chosen for their ability to participate in hydrogen bonding. While pAEMA contains an amide and an amine in the repeat units, pHEMA contains an ester and a hydroxyl. Figure 11 shows the spectra of each polymer alone as well as each polymer mixed with the VSV analyte and the fingerprint spectrum of the VSV alone. The signals are overall stronger for the measurements containing pAEMA. There are also notable differences between the pAEMA alone and the pAEMA mixed with the VSV, whereas the VSV and pHEMA mixture is nearly identical to the pHEMA alone. The primary detectable changes are to the peak intensity ratios. While the ideal situation would be the appearance of strong new VSVspecific peaks, the method of using the pAEMA as an affinity agent was worth further exploration since it may allow multiplex detection of viruses of various sizes. The pAEMA alone is clearly a stronger scatterer than the VSV, though the VSV contains some aromatic structures from the presence of many amino acids comprising the surface glycoproteins. The VSV structure is complex, and its relative distance from the FON surface as compared to the covalently bound polymer leads to lower scattering signals. The polymers used in this study both have multiple polarizable bonds, such as between carbon, oxygen, nitrogen, and hydrogen, in their repeat units, which can give relatively large Raman signals. pHEMA has fewer peaks than the pAEMA and thus has more spectral overlap than the pAEMA with the VSV. Overall, the higher signals of pAEMA and greater visual differences of the mixture from the polymer alone and as compared to the VSV alone reveal pAEMA as the more promising polymer affinity agent

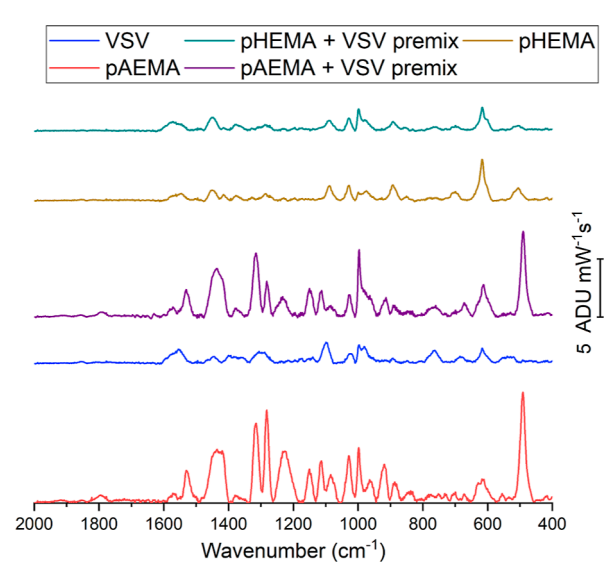


Figure 11. Determining whether pAEMA or pHEMA is the better polymer affinity agent for VSV. The pAEMA + VSV mix is colored purple (middle). pAEMA is in red (bottom). pHEMA is olive and pHEMA mixed with VSV is teal (top). VSV is in blue. pHEMA + VSV is very similar to pHEMA alone. pAEMA + VSV has more differences from both the VSV and the pAEMA.

for this work, and thus all further affinity agent-based studies were performed using this pAEMA.

Interactions between the pAEMA and the VSV are understood in the context of the previously characterized pAEMA spectrum and modeling. 13 Several peaks present in the pAEMA spectrum disappear or significantly decrease in the presence of VSV: delocalized H bending at ~1525 cm⁻¹ shift, C-C-N asymmetric stretch and H associated vibrations at ~1310 cm⁻¹ shift, amine H-vibrations at ~1225 cm⁻¹ shift, and bending and twisting of the secondary amine nitrogen at \sim 500 cm⁻¹ shift. These all stem from the repeat unit of the polymer and suggest potential points of intermolecular interaction with the VSV. As most of these spectral changes are associated with the nitrogen sites and their associated hydrogens, it can be reasoned that the polymer and virus interact through H-bonding. Two potential new peaks also arise from the pAEMA mixed with the VSV spectrum: one around the 700 cm⁻¹ shift and the other around the 760 cm⁻¹ shift. The former is hypothesized to be associated with $C\!-\!S$ stretching and the latter with Trp ring breathing, 28 both part of the surface glycoprotein of the VSV. Many of the other peaks in the mixed spectra could have contributions from both the polymer and analyte, and many undergo line shape changes. Overall, the spectral changes show that the pAEMA and VSV interact and that the analyte is potentially detectable but that the polymer occludes much of the VSV character and complicates the interpretation of spectra.

When the premixing of pAEMA and VSV was tested over a wide range of concentrations (the range tested for the physical entrapment of the analyte), the signals were found to be insensitive to the concentration of analyte present (Figure 12). No linear relationship was found for any of the Raman shifts. This is further evidence that the polymer is the primary contributor to the spectra and is occupying the majority of the Raman-enhancing electromagnetic fields and physically blocking the VSV from much of the FON surface and hotspots. The decay of field enhancement inherent to SERS is the most likely

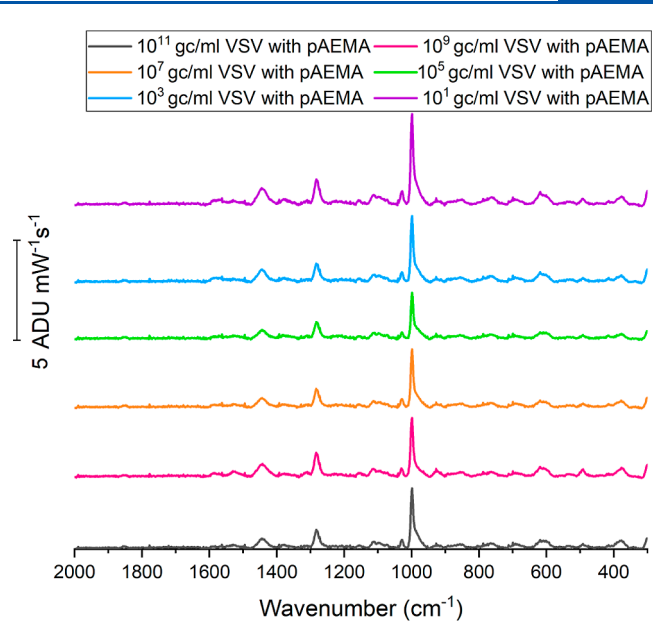


Figure 12. pAEMA premixed with VSV over a range of concentrations from 10¹¹to 10¹ genetic copies/mL. The highest concentration is at the bottom in black, and each spectrum is diluted 100 times from the spectrum below it. There is not a clear dependence on the concentration for the intensities of any of the main peaks.

explanation for the discrepancy between physical entrapment and polymer-enabled capture. By adding a polymer that binds to the gold surface of the FON, there is potential competition introduced for occupation of the enhanced zone proximal to the substrate surface between the analyte and the affinity agent.

4. CONCLUSIONS

In this study, two unconventional methods for the detection of the virus analyte VSV with SERS were explored. First, substrates with VSV-sized gaps and plasmonic properties in alignment with the wavelength of laser excitation were optimized for the physical entrapment of VSV on their surfaces. After the characterization of a fingerprint spectrum for VSV, a wide range of concentrations were successfully detected down to 10¹ genetic copies per milliliter and exhibited a linear relationship to the logarithm of the concentration for the 986 cm⁻¹ shift Raman band. Then, the detection of two additional virus-like particles was explored. Electron microscopy further supported the hypothesis that the viruses were localized in the gaps between the template spheres of the substrate surface for all three analytes. Distinctive Raman fingerprints were also obtained for the other virus-like particles. Then, two nonspecific linear polymer affinity agents were utilized for the capture of VSV for SERS detection. The VSV signal was largely overtaken by the polymer signal, though it was still discernible through PCA. Overall, the physical entrapment method was preferable both for its simplicity and its potential for quantitative analysis. It additionally holds promise for the detection of a wide range of bioanalytes within an accommodating size range, with the possibility of multiplex detection, as demonstrated by the detection of AAV and VLP-N5213 virus-like particles.

ASSOCIATED CONTENT

Supporting Information

The Supporting Information is available free of charge at https://pubs.acs.org/doi/10.1021/acs.analchem.4c01117.

Polymer synthesis details and characterization data; gold film deposition data; additional calibration curve; table of additional potential analytes; PCA for VSV, VLP-N5213, AAV, and mixtures of the analytes; spectra for intra- and intersubstrate reproducibility data; table of reproducibility figures of merit; and polymer concentration study results (PDF)

AUTHOR INFORMATION

Corresponding Author

Christy L. Haynes — Department of Chemistry, University of Minnesota, Minneapolis, Minnesota 55455, United States; orcid.org/0000-0002-5420-5867; Email: chaynes@umn.edu

Authors

Cassandra L. Wouters — Department of Chemistry, University of Minnesota, Minneapolis, Minnesota 55455, United States; orcid.org/0000-0002-4806-7007

Mahmoud Matar Abed – Department of Chemistry, University of Minnesota, Minneapolis, Minnesota 55455, United States

Timmy B. Nguyen — Department of Chemistry, University of Minnesota, Minneapolis, Minnesota 55455, United States; orcid.org/0009-0001-8484-4360

Clarice E. Froehlich – Department of Chemical Engineering and Materials Science, University of Minnesota, Minneapolis, Minnesota 55455, United States; orcid.org/0000-0001-8862-785X

Punarbasu Roy — Department of Chemistry, University of Minnesota, Minneapolis, Minnesota 55455, United States; orcid.org/0000-0001-8937-7856

Theresa M. Reineke — Department of Chemistry, University of Minnesota, Minneapolis, Minnesota 55455, United States; orcid.org/0000-0001-7020-3450

Complete contact information is available at: https://pubs.acs.org/10.1021/acs.analchem.4c01117

Notes

The authors declare no competing financial interest.

ACKNOWLEDGMENTS

The authors would like to acknowledge funding from Boehringer Ingelheim. The contributions by C.W. and C.F. are based upon work supported by the National Science Foundation Graduate Research Fellowship Program (grants 1839286 and 2237827, respectively). T.B.N. acknowledges funding from the University of Minnesota NSF REU program (grant CHE-1851990). P.R. and T.M.R. acknowledge partial funding of this work from NSF DMR-1904853. The authors would like to thank Dr. Yoo-Chun Kim for helpful discussion and VSV samples and Dr. Rebeca Rodriguez and Dr. Victoria Szlag for precedent work. Parts of this work were carried out in the Characterization Facility, University of Minnesota, a member of the NSF-funded Materials Research Facilities Network (www.mrfn.org) via the MRSEC program (award no. DMR-2011401). Portions of this work were conducted in the Minnesota Nano Center and the Nanostructural Materials and

Processes (NMP) program of IPRIME, which are supported by the National Science Foundation through the National Nanotechnology Coordinated Infrastructure (NNCI) under award no. ECCS-2025124.

REFERENCES

- (1) Bishnoi, S.; Tiwari, R.; Gupta, S.; Byrareddy, S. N.; Nayak, D. *Viruses* **2018**, *10* (2), 90.
- (2) Cassedy, A.; Parle-McDermott, A.; O'Kennedy, R. Front. Mol. Biosci. 2021, 8, 637559.
- (3) Bantz, K. C.; Meyer, A. F.; Wittenberg, N. J.; Im, H.; Kurtuluş, O...; Lee, S. H.; Lindquist, N. C.; Oh, S.-H.; Haynes, C. L. *Phys. Chem. Phys.* **2011**, *13* (24), 11551–11567.
- (4) Ambartsumyan, O.; Gribanyov, D.; Kukushkin, V.; Kopylov, A.; Zavyalova, E. *Int. J. Mol. Sci.* **2020**, *21* (9), 3373.
- (5) Krause, M.; Radt, B.; Rösch, P.; Popp, J. J. Raman Spectrosc. **2007**, 38 (4), 369–372.
- (6) Münchberg, U.; Rösch, P.; Bauer, M.; Popp, J. Anal. Bioanal. Chem. 2014, 406 (13), 3041-3050.
- (7) Caglayan, M. G.; Kasap, E.; Cetin, D.; Suludere, Z.; Tamer, U. *Microchim. Acta* **2017**, *184* (4), 1059–1067.
- (8) Saviñon-Flores, F.; Méndez, E.; López-Castaños, M.; Carabarin-Lima, A.; López-Castaños, K. A.; González-Fuentes, M. A.; Méndez-Albores, A. *Biosensors* **2021**, *11* (3), 66.
- (9) Jones, R. R.; Hooper, D. C.; Zhang, L.; Wolverson, D.; Valev, V. K. Nanoscale Res. Lett. 2019, 14 (1), 231.
- (10) Smith, E.; Dent, G. Surface Enhanced Raman Scattering and Surface Enhanced Resonance Raman Scattering. In *Modern Raman Spectroscopy*; Wiley, 2019; pp 119–149..
- (11) Haynes, C. L.; Van Duyne, R. P. J. Phys. Chem. B 2001, 105 (24), 5599-5611.
- (12) Huang, J.; He, Z.; Liu, Y.; Liu, L.; He, X.; Wang, T.; Yi, Y.; Xie, C.; Du, K. Appl. Surf. Sci. **2019**, 478, 793–801.
- (13) Szlag, V. M.; Jung, S.; Rodriguez, R. S.; Bourgeois, M.; Bryson, S.; Schatz, G. C.; Reineke, T. M.; Haynes, C. L. *Anal. Chem.* **2018**, *90* (22), 13409–13418.
- (14) Styles, M. J.; Rodriguez, R. S.; Szlag, V. M.; Bryson, S.; Gao, Z.; Jung, S.; Reineke, T. M.; Haynes, C. L. J. Raman Spectrosc. 2021, 52 (2), 482–490.
- (15) Willets, K. A.; Van Duyne, R. P. Annu. Rev. Phys. Chem. 2007, 58 (1), 267-297.
- (16) Suresh, V.; Ding, L.; Chew, A. B.; Yap, F. L. ACS Appl. Nano Mater. 2018, 1 (2), 886–893.
- (17) Liu, L.; Zhang, Q.; Lu, Y.; Du, W.; Li, B.; Cui, Y.; Yuan, C.; Zhan, P.; Ge, H.; Wang, Z.; Chen, Y. AIP Adv. 2017, 7 (6), 065205.
- (18) Jeon, T. Y.; Kim, D. J.; Park, S.-G.; Kim, S.-H.; Kim, D.-H. Nano Converg. 2016, 3 (1), 18.
- (19) Chen, Y.; Bai, X.; Su, L.; Du, Z.; Shen, A.; Materny, A.; Hu, J. Sci. Rep. 2016, 6 (1), 19173.
- (20) Chang, C.-W.; Liao, J.-D.; Shiau, A.-L.; Yao, C.-K. Sens. Actuators B Chem. 2011, 156 (1), 471–478.
- (21) Durmanov, N. N.; Guliev, R. R.; Eremenko, A. V.; Boginskaya, I. A.; Ryzhikov, I. A.; Trifonova, E. A.; Putlyaev, E. V.; Mukhin, A. N.; Kalnov, S. L.; Balandina, M. V.; Tkachuk, A. P.; Gushchin, V. A.; Sarychev, A. K.; Lagarkov, A. N.; Rodionov, I. A.; Gabidullin, A. R.; Kurochkin, I. N. Sens. Actuators B Chem. 2018, 257, 37–47.
- (22) Szlag, V. M.; Rodriguez, R. S.; Jung, S.; Bourgeois, M. R.; Bryson, S.; Purchel, A.; Schatz, G. C.; Haynes, C. L.; Reineke, T. M. *Mol. Syst. Des. Eng.* **2019**, *4* (5), 1019–1031.
- (23) Rodriguez, R. S.; Szlag, V. M.; Reineke, T. M.; Haynes, C. L. *Mater. Adv.* **2020**, *1* (9), 3256–3266.
- (24) Semsarilar, M.; Perrier, S. Nat. Chem. 2010, 2 (10), 811-820.
- (25) Sheehy, G.; Picot, F.; Dallaire, F.; Ember, K. J.; Nguyen, T.; Petrecca, K.; Trudel, D.; Leblond, F. *J. Biomed. Opt.* **2023**, 28 (2), 025002.
- (26) Motulsky, H. J.; Brown, R. E. BMC Bioinf. 2006, 7 (1), 123.
- (27) Ge, P.; Tsao, J.; Schein, S.; Green, T. J.; Luo, M.; Zhou, Z. H. Science **2010**, 327 (5966), 689-693.

- (28) Francis, D.; Fateley, W.; Bentley, F. Characteristic Raman Frequencies of Organic Compounds; John Wiley & Sons, Inc.: New York, 1974.
- (29) Jeetendra, E.; Ghosh, K.; Odell, D.; Li, J.; Ghosh, H. P.; Whitt, M. A. J. Virol. 2003, 77 (23), 12807–12818.
- (30) Sarychev, A. K.; Sukhanova, A.; Ivanov, A. V.; Bykov, I. V.; Bakholdin, N. V.; Vasina, D. V.; Gushchin, V. A.; Tkachuk, A. P.; Nifontova, G.; Samokhvalov, P. S.; Karaulov, A.; Nabiev, I. *Biosensors* **2022**, *12* (5), 300.
- (31) Huang, J.; Wang, C.; Wang, P.; Mo, W.; Zhou, M.; Le, W.; Qi, D.; Wei, L.; Fan, Q.; Yang, Y.; Ni, S.; Wu, Y.; Feng, Y.; Wang, X.; Zhao, Z.; He, Z.; Zhang, H.; Xue, P.; Ren, B.; Ren, L.; Pan, M.; Du, K. ACS Appl. Mater. Interfaces 2023, 15 (44), 50742–50754.
- (32) Dollish, F.; Fateley, W.; Bentley, F. Appendix 1: Charateristic Raman Frequencies. In *Characteristic Raman Frequencies of Organic Compounds*; John Wiley & Sons, Inc., 1974; pp 284–291.
- (33) Madzharova, F.; Heiner, Z.; Kneipp, J. J. Phys. Chem. C 2017, 121 (2), 1235-1242.
- (34) Arnaout, R.; Lee, R. A.; Lee, G. R.; Callahan, C.; Yen, C. F.; Smith, K. P.; Arora, R.; Kirby, J. E. bioRxiv 2020.
- (35) Murray, C. A. Molecule-Silver Separation Dependence. In Surface Enhanced Raman Scattering; Chang, R. K., Furtak, T. E., Eds.; Springer US: Boston, MA, 1982; pp 203–221...